Atomic collapse in disordered graphene quantum dots

Mustafa Polat* and A. D. Güçlü
Department of Physics, Izmir Institute of Technology, 35430 Urla, Izmir, Turkey

(Received 13 August 2020; revised 2 November 2020; accepted 5 November 2020; published 16 November 2020)

In this paper, we numerically study a Coulomb impurity problem for interacting Dirac fermions restricted in disordered graphene quantum dots. In the presence of randomly distributed lattice defects and spatial potential fluctuations, the response of the critical coupling constant for atomic collapse is mainly investigated by local density of states calculations within the extended mean-field Hubbard model. We find that both types of disorder cause an amplification of the critical threshold. As a result, up to a 34% increase in the critical coupling constant is reported. This numerical result may explain why the Coulomb impurities remain subcritical in experiments, even if they are supercritical in theory. Our results also point to the possibility that atomic collapse can be observed in defect-rich samples such as Ar^+ ion bombarded, He^+ ion irradiated, and hydrogenated graphene.

DOI: 10.1103/PhysRevB.102.174204

I. INTRODUCTION

Quantum electrodynamics predicts that the $1S_{1/2}$ state is stable only up to a critical nuclear charge $Z_c \sim 172$; otherwise, the formerly bound state becomes a resonant state [1]. In spite of its long-standing history [2], the collapse of the vacuum is far from being proven in experiments performed with real atoms [3]. However, graphene reduces the critical threshold to $Z_c \gtrsim 1$ through a larger fine-structure constant $\alpha = 2.2/\kappa$ [4,5], where κ is the dielectric constant. Therefore, the idea of creating an artificial supercritical atom with a smaller critical valence charge has received considerable experimental attention [6–10]. In the condensed-matter analog, Dirac fermions form the vacuum itself, and the Coulomb impurity acts as a nucleus that couples to the vacuum by means of a dimensionless coupling strength $\beta = Z\alpha$ [11]. When β exceeds a critical coupling constant β_c, the lowest-energy electron state first turns into a quasibound state (QBS) [4], which corresponds to the $1S_{1/2}$ state of the impurity, and an infinite number of QBSs can appear for massless fermions, depending on the value of β [5]. The critical coupling constant is estimated to be $\beta_c = 0.5$ for a vacuum consisting of noninteracting massless Dirac fermions [4,5], and it remains the same when these fermions are confined in smaller-sized graphene quantum dots (GQDs) [12,13]. A further extension of the problem takes electron interactions into account [14,15] for which this critical value is renormalized to $\beta_c = 0.6$ due to off-site Coulomb repulsion among Dirac particles [13]. However, until now, all theoretical calculations have assumed disorder-free graphene by ignoring the experimental facts [16,17], and the question of effects of imperfections on atomic collapse in graphene has not been addressed yet.

Atomic scale defects [18,19] and the intercalation of hydrogen (H) atoms [20–22] may arise during the growth process, and these defects lead to an imperfect honeycomb lattice [23,24]. Furthermore, such a deformed vacuum can fluctuate in response to spatial charge inhomogeneities caused by the substrate [25,26]. To find the ambiguous consequences of these distortions beyond the conventional perspective of the theory, the hexagonal GQDs with armchair edges [27] could provide a practical playground. These GQDs serve as a bridge between the finite-size samples and bulk graphene thanks to their special band gap characteristics [27,28], and a sufficiently large number of them is enough to observe atomic collapse, as evidenced by transmission coefficients of the $1S_{1/2}$ state [13]. The latter could help in finding solutions to such complex problems via exact diagonalization of the Hamiltonian, even in the case of interacting fermions.

In this paper, the critical threshold is studied by placing the Coulomb impurity at the center of disordered hexagonal GQDs. Deviations from perfection in the vacuum are intentionally created by (i) randomly distributed point vacancies with different concentrations and (ii) electron-hole puddles induced by Gaussian impurities. We find strong dependence of the critical threshold on both types of disorder, leading to up to a 34% increase in the critical coupling constant.

The rest of this paper is organized as follows. In Sec. II computational models are introduced. The effects of both point vacancies and charge inhomogeneities on the critical threshold are discussed in Sec. III, and Sec. IV consists of our conclusions.

II. COMPUTATIONAL MODELS

The extended mean-field Hubbard model is employed to study the π_z dynamics, and its Hamiltonian reads

$$H_{\mathrm{MFH}} = t\sum_{\langle ij\rangle\sigma}(c^{\dagger}_{i\sigma}c_{j\sigma} + \mathrm{H.c.}) + U\sum_{i\sigma}\left(\langle n_{i\bar{\sigma}}\rangle - \frac{1}{2}\right)n_{i\sigma} + \sum_{ij}V_{ij}(\langle n_j\rangle - 1)n_i - \hbar v_{\mathrm{F}}\beta\sum_{i\sigma}\frac{c^{\dagger}_{i\sigma}c_{i\sigma}}{r_i}, \quad (1)$$

*mustafapolat@iyte.edu.tr

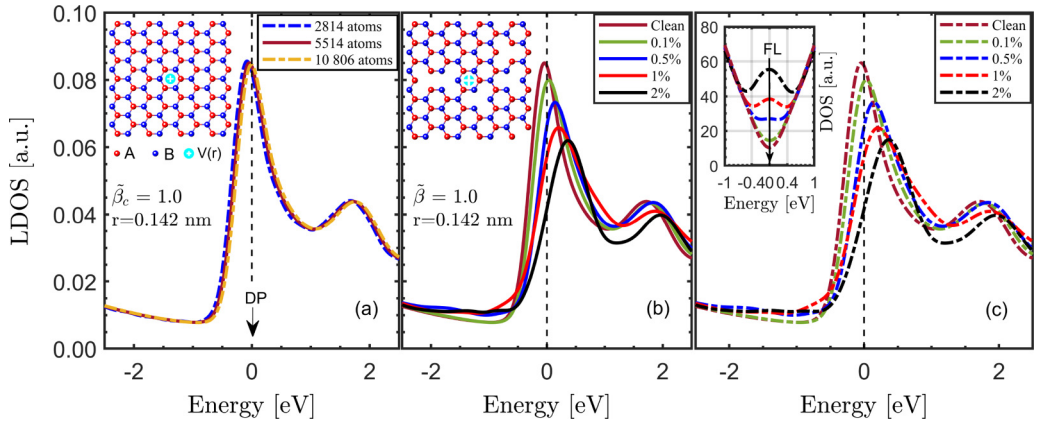

FIG. 1. LDOS spectra at the impurity site for (a) 2814, 5514, and 10 806 atoms, (b) spin-up QBS families, and (c) spin-down QBS families in the presence of finite defect densities. Insets illustrate zoomed portions of (a) perfectly ordered and (b) disordered lattices with a central Coulomb impurity. The inset in (c) is the averaged spin-down DOS that marks the FL at $\tilde{\beta} = 0$.

where the first term describes the tight-binding Hamiltonian with a hopping amplitude of $t = -2.8$ eV in which the operator $c^{\dagger}_{i\sigma}$ ($c_{i\sigma}$) creates (annihilates) an electron with spin σ at lattice site i. $U = 16.52/\kappa$ eV is the on-site Coulomb repulsion [28], where $\kappa = 6$ is equivalent to that of the SiO_2 substrate under the effects of interband polarization [29]. $\langle n_{i\sigma}\rangle$ is the spin-dependent expectation value of electron densities, and $n_{i\sigma}$ is the spin-dependent number operator. The third term, V_{ij}, is associated with the off-site Coulomb repulsion, which is set to be $8.64/\kappa$ eV, $5.33/\kappa$ eV, and $27.21/\kappa d_{ij}$ eV for the nearest-neighbor, next-nearest-neighbor, and remote atomic sites, respectively [28,30]. d_{ij} is the distance between sites i and j at relatively large distances, and it is in atomic units. The last term represents the Coulomb impurity placed at the origin of the coordinate system, where r_i is the distance between the impurity and site i. $\nu_F \approx 1 \times 10^6$ m/s is the Fermi velocity.

Atomic vacancies with concentrations of 0.1%, 0.5%, 1%, and 2%, which refer to the ratio of the number of point vacancies N_{vac} to that of the lattice sites N, are created by randomly and equally removing the two sublattices, A (50%) and B (50%), of the bipartite lattice [31]. For a 1% concentration of carbon vacancies, the electron-hole puddles are created by the superposition of contributions of randomly distributed Gaussian impurities [32] with a total number of $N_{imp} = 16$, i.e., the impurity concentration $n_{imp} = 1.1 \times 10^{13}$ cm^{-2}. The Gaussian potential at a position $\mathbf{r}_n$ can be written as follows: $V_i = \sum_{n=1}^{N_{imp}} \Delta_n \exp[-|\mathbf{r}_i - \mathbf{r}_n|^2/(2\xi^2)]$, where Δ is the impurity strength, and the impurity correlation length is taken to be $\xi = 10a$ ($a = 0.142$ nm is the C-C distance) [33]. Half of these impurities are chosen to be positive, and the other half are chosen to be negative with the help of Δ, which randomly fluctuates within three different intervals: (i) $|\Delta| < 0.1t$, (ii) $|\Delta| < 0.3t$, and (iii) $|\Delta| < 0.5t$.

The local density of states (LDOS) [5] is experimentally accessible through a scanning tunneling microscope (STM) [7] and is calculated by $N(E, r) = \sum_i |\Psi_i(r)|^2 \delta(E - E_i)$, where $\Psi(r)$ is the normalized wave function, the energy E is identical to the applied bias voltage in STM measurements, and E_i is the eigenenergy of the ith state. The LDOS is the spatially resolved density of states (DOS), which is calculated by summing the discrete energy levels of the GQDs at a set of radial distances from the impurity, ranging from $r = 0.142$ nm up to $r = 1.136$ nm. The summations are performed by using a Gaussian membership function with a standard deviation of $\sigma = 0.2$ eV in a linearly spaced energy interval $E \in [-2.5, 2.5]$. Since the effects of random disorders may differ from atom to atom, these calculations are separately carried out for each individual atom at the predefined radial distances, and this is repeated in ten random disorder distributions for each of the above configurations [34]. Finally, the LDOS spectra per lattice site at various distances are extracted by averaging over these samples.

III. RESULTS AND DISCUSSION

It can be useful to discuss the effect of the vacuum size from a different perspective before proceeding to the disordered cases. Pristine hexagonal GQDs that differ in size are created, and their discrete energy levels are summed over at the impurity site $r = 0.142$ nm, as described above. Although such a sum corresponding to a family of QBSs is not necessary for perfect vacuums, it will provide a considerable advantage in the following sections. All supercritical states are sequentially arranged within this family, which contains the $1S_{1/2}$ state as the first component [5]. Atomic collapse occurs when this sharp peak in the electronic LDOS crosses just below the Dirac point (DP) [7], which will be the energy origin in our calculations due to the formation of spatially extended resonances at the negative energies [12]. Meanwhile, the Fermi level (FL) moves down starting from the energy origin as the coupling strength is increased within the half-filled model [12,13]. To avoid too cumbersome notation, the critical coupling constant of the families of QBSs is represented by $\tilde{\beta}_c$, and only the response of the spin-up Dirac fermions is studied for perfect vacuums due to the presence of a spin-independent central potential. The spin-up QBS families at the impurity site are shown in Fig. 1(a) for perfect GQDs consisting of 2814, 5514, and 10 806 carbon atoms. All families are pinned just below the DP at $\tilde{\beta}_c = 1.0$, revealing that the effect of the Coulomb impurity is the same for all these GQDs, and the

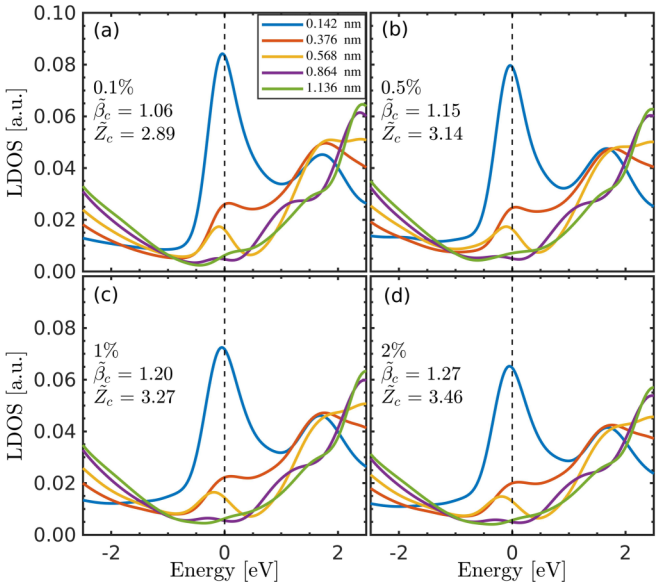

FIG. 2. Defect-induced increase in the critical coupling constant $\tilde{\beta}_c$ for concentrations of 0.1% in (a), 0.5% in (b), 1% in (c), and 2% in (d). Here spin-up and spin-down QBS families exactly overlap, and the different colored lines represent the corresponding radial distances from the impurity.

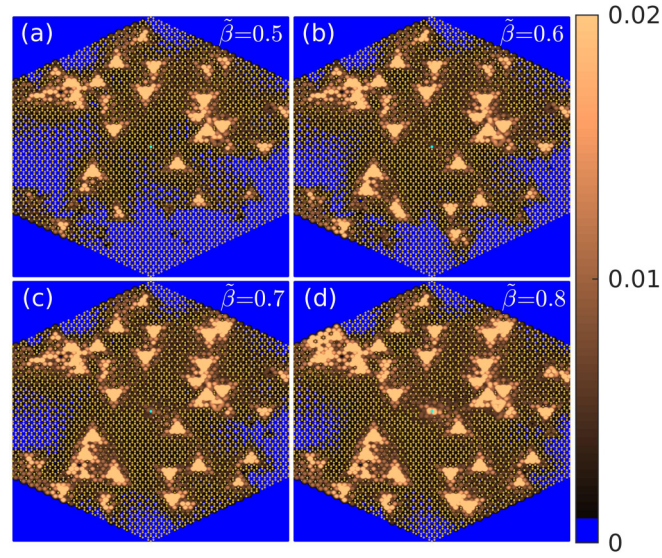

FIG. 3. Response of the empty defect states below the DP to the Coulomb field for a representative sample with 1% defect density. Their spatial distributions are shown in (a)–(d) for $\tilde{\beta} = 0.5$, 0.6, 0.7, and 0.8, respectively. Upward (downward) triangles belong to the unoccupied spin-up (spin-down) vacancy-induced states. As is clear from (d), the $1S_{1/2}$ state is formed at the center of the QD marked by green dots.

critical bare valence charge is calculated to be $\tilde{Z}_c \approx 2.73$ by taking $\kappa = 6$.

When point defects are evenly distributed between the sublattices, i.e., A (50%) and B (50%), the FL continues to stay at the energy origin in the absence of impurity [35–37], as shown in the inset of Fig. 1(c). In fact, the FL is the same for both the perfect and disordered cases, which validates the previous discussion on the DP and the FL in our defect configurations when $\tilde{\beta}$ is turned on. As for the spin symmetry, it is naturally broken in the disordered lattices [31]. However, there is no difference between the spin-up and spin-down families near $\tilde{\beta}_c$, as shown in Figs. 1(b) and 1(c), respectively. As is clear from these two figures, all QBS families at the impurity site retreat from the DP depending on the concentrations of these defects, which are randomly distributed in the GQD lattice consisting of 5514 atoms in the pristine case. Figures 1(b) and 1(c) point out that $\tilde{\beta} = 1.0$ is no longer a critical coupling constant, and it is the first effect of point defects on atomic collapse.

These families transit from above to the edge of the DP at different $\tilde{\beta}_c$, which is evident in Figs. 2(a)–2(d). The critical coupling constant gradually increases in proportion to the defect densities and reaches $\tilde{\beta}_c = 1.27$ for random dilution at 2% [see Fig. 2(d)]. Actually, these defects are ubiquitous in the crystal structure [23]. For example, the Raman spectrum has an $\sim 0.5G$ to $2D$ intensity ratio for the high-quality graphene monolayer grown by chemical vapor deposition (CVD) [38], and this ratio indicates that there is a finite defect density in graphene. As is clear from our numerical results, these structural peculiarities can cause an increase in the critical threshold. On the other hand, the spectral shapes of all QBS families are the same as that of the defect-free case, especially in the vicinity of the impurity. It can be inferred that atomic collapse can be similarly observed in the imperfect lattices with the help of a higher valance charge.

In the half-filled Hubbard model, the lowest-energy states in the conduction band are unoccupied vacancy-induced states whose energies are in the range $0 < E < 0.4$ eV for the 1% defect concentration [see the global DOS in the inset of Fig. 1(c)]. As $\tilde{\beta}$ is increased, these states successively dive into the negative energies. However, there is no explicit crossing from the higher-energy conduction states within the energy spectrums. Therefore, of particular interest are these merging states below the DP, and their total probability density is calculated by $p(r) = (1/2)[\sum_{E<0} |\Psi(r)|^2 - \sum_{E<E_F} |\Psi(r)|^2]$, in which both spin components are included. For a representative sample, $p(r)$ is projected into space at different coupling constants, ranging from $\tilde{\beta} = 0.5$ up to $\tilde{\beta} = 0.8$. Figures 3(a)–3(d) clearly show that whenever defect states dive just below the DP, they are localized around the missing atoms by preserving their characteristic triangular shapes and then demonstrate a striking stability against the Coulomb impurity. On the other hand, the weight of the probability density around the impurity progressively increases, but there is no formation of the first supercritical state at $\tilde{\beta} = 0.5$ or at $\tilde{\beta} = 0.6$, which are the critical coupling constants of the $1S_{1/2}$ state for the noninteracting [5] and interacting [13] fermions in a clean vacuum, respectively. Finally, the $1S_{1/2}$ state [39] appears at $\tilde{\beta} = 0.8$, despite not being a direct contribution of the bulk states to $p(r)$. Such a formation of the $1S_{1/2}$ state is presumably due only to the hybridized components of the diving defect states, and the defect-induced increases in Figs. 2(a)–2(d) actually originate from the formation mechanism of the $1S_{1/2}$ state.

Prior to the collapse experiments [6–9], monolayer graphene is grown by CVD and then is transferred onto a

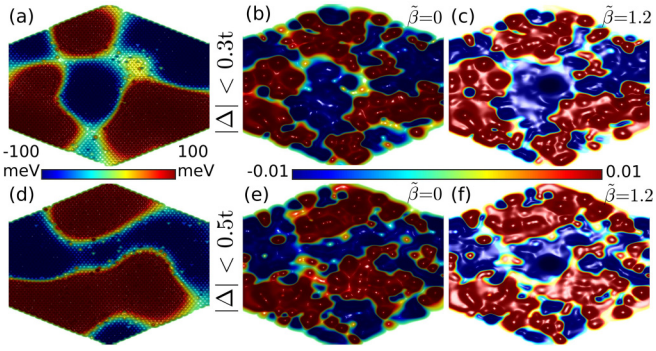

FIG. 4. (a) Averaged potential fluctuations for $|\Delta| < 0.3t$ (only $|\Delta|$ are averaged); (b) the total electron-hole puddles accordingly are formed at $\tilde{\beta} = 0$, and (c) the reformation of these charge puddles is formed at $\tilde{\beta} = 1.2$. (d)–(f) The same as (a)–(c), but now for $|\Delta| < 0.5t$.

hexagonal boron nitride (hBN) flake placed on a SiO_2/Si substrate. To model the spatial potential fluctuations caused by such a substrate, we randomly distributed Gaussian impurities for the set of vacuum disordered by the 1% concentration of carbon vacancies. The averaged potential landscapes of $|\Delta| < 0.3t$ and $|\Delta| < 0.5t$ are shown in Figs. 4(a) and 4(d), respectively. The resulting electron-hole puddles of both spin components show that the electron puddles (red) appear in the positive potential regions, whereas the hole puddles (blue) manifest themselves in the negative potential regions, as can be seen in Fig. 4(b) for $|\Delta| < 0.3t$ and Fig. 4(e) for $|\Delta| < 0.5t$. As $\tilde{\beta}$ is turned on, the charge inhomogeneities rearrange themselves under the effect of the Coulomb potential. For example, at $\tilde{\beta} = 1.2$, the electron-hole puddles of $|\Delta| < 0.3t$ and those of $|\Delta| < 0.5t$ are mapped in Figs. 4(c) and 4(f), respectively. Even if there is no significant change in the positions of the hole puddles formed at the distances away from the center, those close to the center leave their positions and are centered around the stronger Coulomb impurity. As will be seen below, such a reformation has a significant effect on the critical threshold.

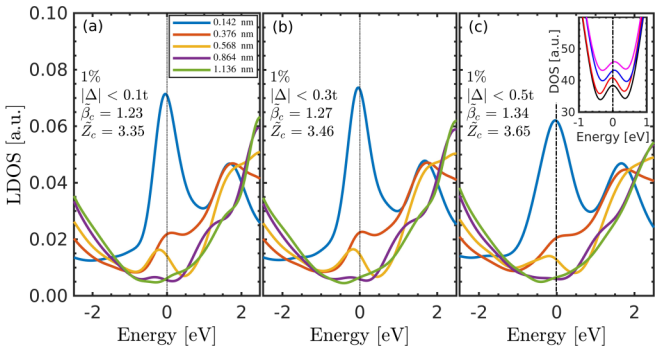

FIG. 5. The effect of electron-hole puddles on the critical threshold in (a)–(c), which is the same for both spin components. The inset in (c) shows averaged total DOS at $\tilde{\beta} = 0$, where black, red, blue, and purple lines represent $\Delta = 0$, $|\Delta| < 0.1t$, $|\Delta| < 0.3t$, and $|\Delta| < 0.5t$, respectively. For the sake of simplicity, a space between these lines is intentionally added.

LDOS spectra in Figs. 5(a)–5(c) are calculated for the spin-up QBS family at the corresponding radial distances, starting from the impurity site. When the positive and negative Gaussian impurities are distributed evenly, the total DOS of the spin-up fermions at $\tilde{\beta} = 0$ clearly reveals that the FL is again around the energy origin for these configurations [see the inset in Fig. 5(c)]. There is no significant shift in the minimum-energy point at $\tilde{\beta} = 0$, allowing us to take the energy origin as the DP for the nonzero values of $\tilde{\beta}$. Similar to the previous cases, whenever the sharp peak enters the negative energy spectrum, the atomic collapse has occurred. The addition of Gaussian impurities causes an increase in the critical threshold from $\tilde{\beta}_c = 1.20$ [Fig. 2(c)] to $\tilde{\beta}_c = 1.34$ [Fig. 5(c)], and the critical valance charge is estimated to be as high as $\tilde{Z}_c = 3.65$. In addition, we also study the point-defect-free GQD consisting of 5514 atoms for ten random distributions of $|\Delta| < 0.5t$, and the critical threshold reaches $\tilde{\beta}_c = 1.10$ (not shown here), which is $\tilde{\beta}_c = 1.0$ [Fig. 1(a)] in its clean case. It can be noted that the increments in the critical threshold are independent of the sign of the substrate-induced potential where the Coulomb impurity is placed and are directly proportional to the strengths of Gaussian impurities. As a result, $\tilde{\beta}_c$ seems to be highly influenced by the disorders within the vacuum itself.

IV. CONCLUSION

In bulk graphene, a series of LDOS measurements performed by a STM revealed that a cluster, composed of four calcium dimers in the charge state of $+1|e|$, is needed to form an infinite family of QBSs at just above the DP (see Fig. 1(D) in Ref. [7]). Therefore, the critical bare valance charge should be slightly greater than $\tilde{Z}_c \gtrsim 4$ in the experiment. Accordingly, the calculated values of $\tilde{Z}_c$ approach that of the experiment, and adding these experimentally relevant factors to the Coulomb impurity problem opens a new route towards such experimental results [6,7]. These findings can be useful in interpreting the experimental results of positively charged Coulomb impurities, even if they exceed the theoretical critical value. The results of this paper can be tested via Ar^+ ion bombarded [40], He^+ ion irradiated [41], and hydrogenated [42] graphene. The latter can be achieved by transferring CVD graphene samples at different H coverages [42] onto a hBN/SiO_2/Si device, which facilities control bias and back-gate voltages. Impurities such as cobalt trimmers [6] and calcium dimers [7,9] can be gathered in a defect-rich region by atomic manipulation of them with the help of STM, and an artificial supercritical atom can be created from these subcritical impurities. Once the DP has been determined, LDOS spectra can be measured at different radial or lateral distances. There should be an increase in the critical threshold due to the partial removal of the π_z states depending on the concentration of H.

ACKNOWLEDGMENTS

This work was supported by the Scientific and Technological Research Council of Turkey (TUBITAK) under 1001 Grant Project No. 116F152.

[1] J. Reinhardt and W. Greiner, Rep. Prog. Phys. **40**, 219 (1977).

[2] W. Greiner, *Relativistic Quantum Mechanics* (Springer, New York, 2000).

[3] T. Cowan, H. Backe, M. Begemann, K. Bethge, H. Bokemeyer, H. Folger, J. S. Greenberg, H. Grein, A. Gruppe, Y. Kido, M. Kluver, D. Schwalm, J. Schweppe, K. E. Stiebing, N. Trautmann, and P. Vincent, Phys. Rev. Lett. **54**, 1761 (1985).

[4] V. M. Pereira, J. Nilsson, and A. H. Castro Neto, Phys. Rev. Lett. **99**, 166802 (2007).

[5] A. V. Shytov, M. I. Katsnelson, and L. S. Levitov, Phys. Rev. Lett. **99**, 246802 (2007).

[6] Y. Wang, V. W. Brar, A. V. Shytov, Q. Wu, W. Regan, H.-Z. Tsai, A. Zettl, L. S. Levitov, and M. F. Crommie, Nat. Phys. **8**, 653 (2012).

[7] Y. Wang, D. Wong, A. V. Shytov, V. W. Brar, S. Choi, Q. Wu, H.-Z. Tsai, W. Regan, A. Zettl, R. K. Kawakami *et al.*, Science **340**, 734 (2013).

[8] J. Mao, Y. Jiang, D. Moldovan, G. Li, K. Watanabe, T. Taniguchi, M. R. Masir, F. M. Peeters, and E. Y. Andrei, Nat. Phys. **12**, 545 (2016).

[9] D. Wong, F. Corsetti, Y. Wang, V. W. Brar, H.-Z. Tsai, Q. Wu, R. K. Kawakami, A. Zettl, A. A. Mostofi, J. Lischner *et al.*, Phys. Rev. B **95**, 205419 (2017).

[10] J. Lu, H.-Z. Tsai, A. N. Tatan, S. Wickenburg, A. A. Omrani, D. Wong, A. Riss, E. Piatti, K. Watanabe, T. Taniguchi *et al.*, Nat. Commun. **10**, 1 (2019).

[11] A. H. Castro Neto, F. Guinea, N. M. R. Peres, K. S. Novoselov, and A. K. Geim, Rev. Mod. Phys. **81**, 109 (2009).

[12] R. Van Pottelberge, M. Zarenia, P. Vasilopoulos, and F. M. Peeters, Phys. Rev. B **95**, 245410 (2017).

[13] M. Polat, H. Sevinçli, and A. D. Güçlü, Phys. Rev. B **101**, 205429 (2020).

[14] R. R. Biswas, S. Sachdev, and D. T. Son, Phys. Rev. B **76**, 205122 (2007).

[15] I. S. Terekhov, A. I. Milstein, V. N. Kotov, and O. P. Sushkov, Phys. Rev. Lett. **100**, 076803 (2008).

[16] A. Hashimoto, K. Suenaga, A. Gloter, K. Urita, and S. Iijima, Nature (London) **430**, 870 (2004).

[17] J. Martin, N. Akerman, G. Ulbricht, T. Lohmann, J. v. Smet, K. Von Klitzing, and A. Yacoby, Nat. Phys. **4**, 144 (2008).

[18] J. C. Meyer, C. Kisielowski, R. Erni, M. D. Rossell, M. Crommie, and A. Zettl, Nano Lett. **8**, 3582 (2008).

[19] F. Banhart, J. Kotakoski, and A. V. Krasheninnikov, ACS Nano **5**, 26 (2011).

[20] K. M. McCreary, A. G. Swartz, W. Han, J. Fabian, and R. K. Kawakami, Phys. Rev. Lett. **109**, 186604 (2012).

[21] W.-X. Wang, Y.-W. Wei, S.-Y. Li, X. Li, X. Wu, J. Feng, and L. He, Phys. Rev. B **97**, 085407 (2018).

[22] K. E. Çakmak, A. Altıntaş, and A. D. Güçlü, Phys. Rev. B **98**, 115428 (2018).

[23] A. Eckmann, A. Felten, A. Mishchenko, L. Britnell, R. Krupke, K. S. Novoselov, and C. Casiraghi, Nano Lett. **12**, 3925 (2012).

[24] S.-Y. Li, Y.-N. Ren, Y.-W. Liu, M.-X. Chen, H. Jiang, and L. He, 2D Mater. **6**, 031005 (2019).

[25] K. M. Burson, W. G. Cullen, S. Adam, C. R. Dean, K. Watanabe, T. Taniguchi, P. Kim, and M. S. Fuhrer, Nano Lett. **13**, 3576 (2013).

[26] H. U. Özdemir, A. Altıntaş, and A. D. Güçlü, Phys. Rev. B **93**, 014415 (2016).

[27] A. D. Güçlü, P. Potasz, and P. Hawrylak, Phys. Rev. B **82**, 155445 (2010).

[28] A. D. Güçlü, P. Potasz, M. Korkusinski, and P. Hawrylak, *Graphene Quantum Dots* (Springer, Berlin, 2014).

[29] T. Ando, J. Phys. Soc. Jpn. **75**, 074716 (2006).

[30] P. Potasz, A. D. Güçlü, and P. Hawrylak, Phys. Rev. B **82**, 075425 (2010).

[31] A. Altıntaş and A. D. Güçlü, Solid State Commun. **281**, 44 (2018).

[32] J. H. Bardarson, J. Tworzydło, P. W. Brouwer, and C. W. J. Beenakker, Phys. Rev. Lett. **99**, 106801 (2007).

[33] Y. Zhang, V. W. Brar, C. Girit, A. Zettl, and M. F. Crommie, Nat. Phys. **5**, 722 (2009).

[34] Consider the case with the 1% defect concentration; we have ten different samples, each with totally random distributions. For each of these samples, we randomly distribute Gaussian impurities with $|\Delta| < 0.1t$. This is also performed for $|\Delta| < 0.3t$ and $|\Delta| < 0.5t$ in the presence of the 1% defect concentration.

[35] V. M. Pereira, F. Guinea, J. M. B. Lopes Dos Santos, N. M. R. Peres, and A. H. Castro Neto, Phys. Rev. Lett. **96**, 036801 (2006).

[36] V. M. Pereira, J. M. B. Lopes Dos Santos, and A. H. Castro Neto, Phys. Rev. B **77**, 115109 (2008).

[37] E. B. Kul, M. Polat, and A. D. Güçlü, Solid State Commun. **322**, 114096 (2020).

[38] X. Li, W. Cai, J. An, S. Kim, J. Nah, D. Yang, R. Piner, A. Velamakanni, I. Jung, E. Tutuc *et al.*, Science **324**, 1312 (2009).

[39] Its shape is exactly the same as the $1S_{1/2}$ state of the defect-free GQDs (not shown here), and this formation is observed for all samples at around $\tilde{\beta} = 0.8$ for random dilution at 1%.

[40] M. M. Lucchese, F. Stavale, E. M. Ferreira, C. Vilani, M. V. d. O. Moutinho, R. B. Capaz, C. A. Achete, and A. Jorio, Carbon **48**, 1592 (2010).

[41] J.-H. Chen, W. G. Cullen, C. Jang, M. S. Fuhrer, and E. D. Williams, Phys. Rev. Lett. **102**, 236805 (2009).

[42] A. Bostwick, J. L. McChesney, K. V. Emtsev, T. Seyller, K. Horn, S. D. Kevan, and E. Rotenberg, Phys. Rev. Lett. **103**, 056404 (2009).